Available online at www.sciencedirect.com
SCIENCE DIRECT
Journal of Power Sources 158 (2006) 663–672
JOURNAL OF POWER SOURCES
www.elsevier.com/locate/jpowsour

Predicting current flow in spiral wound cell geometries

Jan N. Reimers*

E-One Moli Energy (Canada) Ltd., R&D, 20 000 Stewart Crescent, Maple Ridge, BC, Canada V2X 9E7

Received 14 July 2005; received in revised form 2 August 2005; accepted 3 August 2005
Available online 25 October 2005

Abstract

A general method is described for calculating potential, current and heat-power distributions in electrode foils. The resulting theory is suitable for cell designs with an arbitrary number of current collecting tabs. Example calculation results for a three tab cell design with an ohmic stack impedance are shown. Internal mixing currents, a non-uniform stack current distribution, and sharply peaked heat generation near the tabs, are predicted.

Keywords: Foil impedance; Current collection; Heat generation

1. Introduction

Most commercial Li-ion cells consist of layers of foil current collectors, active electrodes, and separator coiled into a spiral geometry, which is often referred to as a *jelly roll*. The jelly roll cell geometry is not unique to the Li-ion chemistry. Emerging from a jelly roll there must be at least two *tabs* (usually metal strips) which are, unfortunately, often *also* referred to as current collectors. During discharge of such a cell, electrical current will flow into the anode tab(s), along the anode foil, across the electrode stack, along the cathode foil, and out the cathode tab(s).

Over the past 20 years great progress has been achieved in understanding the electrical and ionic current flows across the electrode stack of Li-ion, NiMH or lead acid cells. Given a sufficient quality of transport and thermodynamic properties for the electrodes and electrolyte, it is possible to predict the dynamic response of the stack for a given stack design. Having this capability should be an integral part of any cell design engineer's tool kit. The theory and practical implementation of these techniques has been described elsewhere (for a comprehensive review see ref. [1] and references therein).

Much of this work treats the electrode-separator stack using a one dimensional model, the assumption being that the electronic conductivity of the current collector foils is very high in relation to the effective conductivity of the stack. Hence any potential drop in the foils and tabs can be ignored. This is indeed reasonable for many commercial cell designs. However, with recent interest in power optimized cells aimed at, for example, HEV applications, the geometry may be modified to the point where the impedance of foils becomes significant.

Some previous workers in this field have addressed this issue in their models [2–4] for simple tab arrangements (one anode and one cathode tab). The purpose of this work is to outline a practical method for calculation of foil current and potential distributions for the general case, with any number of tabs, located at arbitrary positions along the length of the electrode foils. With commercial cells already on the market using numerous tabs per electrode, this is not just a purely academic issue.

2. Cell geometry

Unfortunately the term *current collector* is often overloaded to refer to both the *tabs* and the electrode *foils*. Since the distinction is important for understanding this work usage of this overloaded term will be avoided. The cell geometry considered in this work is shown schematically in Fig. 1 for a non trivial arrangement of the tabs (two anode and one cathode tab). With the z direction going into the page, the stack layers (foils, electrodes and separator) are in the xz plane. This diagram represents an jelly roll as viewed end on after it has been unwound. The y direction has been greatly magnified for clarity.

* Tel.: +1 604 466 6669; fax: +1 604 466 6600.
E-mail address: janr@molienergy.com.

0378-7753/$ – see front matter © 2005 Elsevier B.V. All rights reserved.
doi:10.1016/j.jpowsour.2005.08.042

Nomenclature

a, b	adjustable parameters in the general solution to the foil potential field equation, determined by external boundary conditions
c	adjustable parameter in the general solution to the foil potential field equation, determined by external boundary conditions (V cm^{-1})
d	adjustable parameter in the general solution to the foil potential field equation, determined by external boundary conditions (V)
i	stack current density (mA cm^{-2})
I	externally applied current (A)
I_A, I_C	anode and cathode foil currents (A)
L	length of the electrodes in the x direction (cm)
n	total number of tabs sticking out of the jelly roll
n_A^i, n_C^i	number of internal tabs on the anode and cathode electrodes
n_A^e, n_C^e	number of external tabs on the anode and cathode electrodes
n_A, n_C	number of tabs (internal *and* external) on the anode and cathode electrodes
n^i, n^e	number of internal and external tabs on all electrodes
O()	higher order terms
q	state of charge in the active stack (A h cm^{-2})
q_A, q_C	heat generation rate in the anode and cathode foils (W cm^{-2})
q_{stack}	heat generation rate in the stack (W cm^{-2})
r_A, r_C	relative foil impedances, $r_A + r_C = 1$
R_A, R_C	length specific anode and cathode foil resistivities (mΩ cm^{-1})
R_{cell}^{fd}	externally observed, finite difference cell impedance (mΩ)
R_{cell}^{diff}	externally observed, differential cell impedance (mΩ)
R_{stack}	effective stack impedance (Ω cm^2)
t	time (s)
T_A, T_C	anode and cathode foil thicknesses (μm)
V_{cell}	externally observed cell voltage (V)
$V_o(q)$	open circuit voltage curve for the active stack (V)
W_A, W_C	anode and cathode foil widths (cm)
x	distance along the length of the electrodes (cm)
y	distance across the stack (μm)
z	distance across the width of the electrodes, or jelly roll height (cm)

Greek letters

α	inverse length scale (cm^{-1})
ϵ^{solid}, ϵ^{pore}	solid and pore volume fractions in an electrode or separator
κ	electrolyte conductivity (S cm^{-1})
ϕ	potential difference across the stack under load (V)
ϕ_A, ϕ_C	anode and cathode foil potentials (V)
ϕ^p	particular solution to the foil potential field equation (V)
ϕ^{left}, ϕ^{right}	solutions to the homogenous foil potential field equation (V)
ρ_A, ρ_C	specific resistivity of the anode and cathode electrode foils (μΩ cm)
σ	electrical conductivity in the solid phase of an electrode (S cm^{-1})

Subscripts

A	anode
C	cathode
j	segment or tab index

The relevance of the jelly roll geometry to this work lies only in the *length* of the electrodes in the x direction. Matters of curvature are not important for the calculation of dc foil current distributions (the dc resistance of a piece of wire does not change when coiled).

Current runs along the foils in the x, or *in-plane,* direction and through the stack in the perpendicular y, or *through-plane,* direction. Following the convention in the cell modeling literature, a positive stack current flows in the same direction as positive ions, from anode to cathode, as indicated by the vertical arrows, and corresponds the discharge of the cell. Along the foils, positive current flows in the positive x direction, as indicated by the horizontal arrows. With these conventions, electron flow in the foils is of course opposite to the current flow. In a real cell the extent of the tabs in the x direction (tab width) is usually $<1\%$ of the total electrode length. Indeed it is the width of the contact points (weld pattern) that is relevant, and this is often significantly narrower than the tab itself. In order to simplify the analysis the contact width of the tabs is considered to be zero. The z direction, going into the page, corresponds to the width of the electrodes or the length/height of the jelly roll. Currents and potentials are assumed to be constant in the z direction. Again this is a very good approximation as long as the tab resistance in negligible in the z direction.

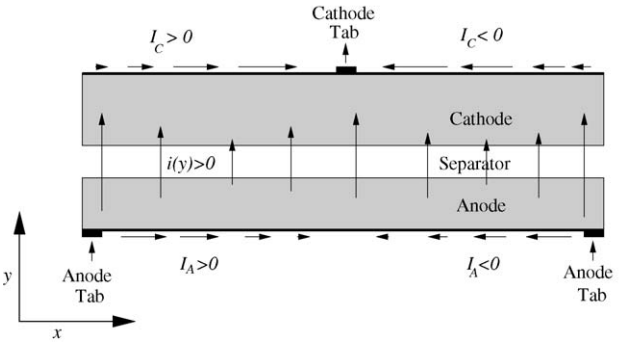

Fig. 1. Schematic cell geometry corresponding to an unwound jelly roll. Black rectangles attached to the foils indicate the position of the tabs.

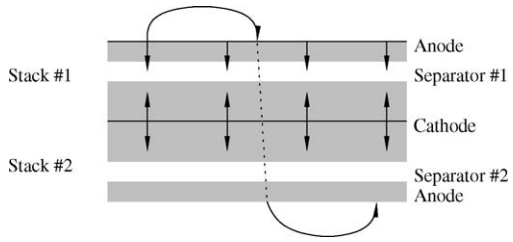

Fig. 2. Current flow geometry for a spiral wound jelly roll with double sided electrodes.

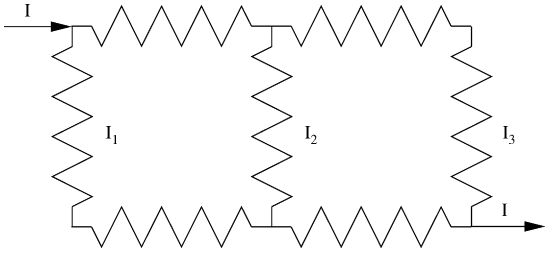

Fig. 3. Instructive resistor network.

Fig. 1 is a simplified version of the real jelly-roll geometry. In commercial cells both electrodes are coated on both sides, which means each foil has two stack directions to send current into. The cell actually has two separate stacks in parallel. Fig. 2 also shows a current path flowing upwards from the anode foil through stack #2, and into the cathode one jelly roll wrap further away. In this work the offset effect will be neglected, which is reasonable if the number of wraps is large. However, the double stack effect must taken into account as will be described below.

Fig. 1 also attempts to show qualitatively, using arrow length, what would be expected regarding the magnitudes of the various currents. In particular the foil currents decrease in magnitude away from the tabs as more and more current makes a right (or left) turn and goes through the stack. What is not so obvious is that the current distribution across the stack is non-uniform, the current is reduced away from the tabs. As will be discussed below, this is actually a transient effect at the beginning of discharge. The situation is analogous to the current flow in the simple resistor network shown in Fig. 3. If all three vertical resistors are of equal value, and the horizontal resistors in any row are equal, one finds that less current flows through the middle resistor $I_2 < I_1 = I_3$.

3. Theory

3.1. Foil current divergence

Where possible units will be written in square brackets, for the various symbols as they are defined. This will hopefully help the reader keep track of absolute, length and area specific currents and resistances. Many expressions are duplicated for anode and cathode. In some cases there are important sign differences between anode and cathode, in which case both expressions will be explicitly written out for clarity.

Ohms law relates the current and potentials in the foil

$$-\frac{\rho_A}{T_A W_A} I_A(x) = -R_A I_A(x) = \nabla\phi_A(x) \tag{1}$$

where for the anode ρ_A is foil resistivity (Ω cm), T_A is the foil thickness (cm), W_A is the foil width (cm), ϕ_A is the potential along the foil (V) and $R_A = \rho_A/T_A W_A$ is the length specific foil resistance ($\Omega\,\mathrm{cm}^{-1}$), with corresponding definitions for the cathode. Note that the possibility of distinct foil widths for anode and cathode is included, this is indeed the case in commercial cells.

One can define the potential across the stack at any point along the foils as

$$\phi(x) = \phi_C(x) - \phi_A(x).$$

Similarly one can define a stack current density i ($\mathrm{A\,cm}^{-2}$). Away from the tabs, detailed current balance in the anode foil gives

$$\nabla I_A(x) = -Wi(x), \quad x \neq x^j. \tag{2}$$

where x^j is the location of the jth tab, and W = minimum $\{W_A, W_C\}$ is the *active* width (usually the cathode is narrower than the anode so $W = W_C$). This just says that away from the tabs, the divergence of the current in the foil is proportional to the flux across the stack at that point. Right at a tab the current is non-analytic, this will be discussed in more detail below. Due to our choice of the current direction in the foils, for the cathode foil current divergence the sign is reversed

$$\nabla I_C(x) = Wi(x), \quad x \neq x^j. \tag{3}$$

3.2. Effective stack impedance

In order to proceed to the next stage, a relationship is required between the stack potential and stack current density. A comprehensive description of this relationship is provided by the one-dimensional stack models described in ref. [1]. Because of diffusion effects and active particle surface reaction kinetics, this relationship is in general non linear:

$$\phi(x) = V_o(q(x)) - R_{stack}(x)i(x) + O(i^2) + \cdots. \tag{4}$$

where $V_o(q)$ (V) is the open circuit voltage (OCV) of the stack, q ($\mathrm{A\,h\,cm}^{-2}$) is the state of charge in the stack, R_{stack} ($\Omega\,\mathrm{cm}^2$) is the effective stack impedance at $i = 0$, and $O(i^2)$ indicates terms of order i^2 or higher. V_o can be measured directly on a full cell at low current, or it can be calculated from the voltage curves of the individual electrodes. In the latter case knowledge of the cell balance is also required.

It is instructive to make an Ohmic approximation and assume R_{stack} is a constant in space and time and higher order terms in (4) are neglected. In this case the mechanics of foil potentials and currents are more easily understood. The general case will be described in Appendix A. When higher order terms are neglected one can invert (4)

$$i(x) = \frac{V_o(q(x)) - \phi(x)}{R_{stack}} \tag{5}$$

A rough estimate for the area specific stack impedance can be obtained from a volume weighted sum of electronic and ion contributions. For one electrode

$$R_{\text{electrode}} \approx T\left(\frac{1}{\epsilon^{\text{solid}}\sigma} + \frac{1}{\epsilon^{\text{pore}}\kappa}\right) \tag{6}$$

where T is the electrode thickness, σ is the electronic conductivity of the solid phase, κ is the conductivity of the electrolyte, and the ϵ's are the corresponding volume fractions. If the volume fraction of inactive materials is negligible then $\epsilon^{\text{solid}} + \epsilon^{\text{pore}} \approx 1$. The wetted separator impedance is similar, but without the solid phase term. Using conductivities from [5,6] for 25 μm separator and 100 μm electrodes, one finds $R_{\text{stack}} \sim 2$–$5\,\Omega\,\text{cm}^2$.

Eq. (6) ignores the effective impedance of the charge transfer reactions at the surface of the active particles. Analytic relations for the effective stack impedance including charge transfer effects have been reported elsewhere [7,3,8]. Using conductivity and exchange current values from ref. [5] for a 100 μm thick electrode, one finds that the charge transfer resistance is on the order of $3\,\Omega\,\text{cm}^2$ per electrode. In total one expects $R_{\text{stack}} \approx 10\,\Omega\,\text{cm}^2$ using this sort of calculation. Measured values for power optimized cells [9] are in the range 30–50 $\Omega\,\text{cm}^2$.

The R_{stack} calculations described above are for one stack sandwich. Since the real cell has two of these in parallel, it sees half the calculated stack impedance. In addition, when interpreting stack impedances for spiral wound cells reported in the literature, these reported numbers are usually for two stacks in parallel.

3.3. Potential equation

In general all currents and potentials are functions of position and time (x and t). For brevity below it is assumed this is implied unless required or otherwise stated. Differentiating (1) and using (2) and doing similarly for the cathode

$$R_{\text{A}} Wi = \nabla^2\phi_{\text{A}},$$
$$-R_{\text{C}} Wi = \nabla^2\phi_{\text{C}}.$$

Subtracting gives

$$\nabla^2\phi_{\text{C}} - \nabla^2\phi_{\text{A}} = \nabla^2\phi = -W(R_{\text{A}} + R_{\text{C}})i. \tag{7}$$

Using (5) one finds

$$\nabla^2\phi = -W(R_{\text{A}} + R_{\text{C}})\frac{V_{\text{o}} - \phi}{R_{\text{stack}}}$$
$$(\nabla^2 - \alpha^2)\phi = -\alpha^2 V_{\text{o}} \tag{8}$$

where

$$\alpha^2 = \frac{W(R_{\text{A}} + R_{\text{C}})}{R_{\text{stack}}} \tag{9}$$

3.4. Segmented solution

Every unique tab position is a point source or sink for current. The degenerate case where two tabs are directly opposite each other (one on the anode and one on the cathode) amounts to only one unique tab position. Tabs at the ends of the electrodes ($x = 0$ or $x = L$) are referred to as external tabs. The x interval between any two neighboring tab positions will be referred to as a *segment*. For example, in Fig. 1 above, the cathode foil has one internal tab and no external tabs, the anode foil has two external tabs and no internal tabs. Both anode and cathode have two segments, one from 0 to $L/2$, and the other from $L/2$ to L. In particular there is a segment boundary on the *anode* directly opposite the cathode tab.

Defining $L_j = x_{j+1} - x_j$ as the length of the foils in the x direction for segment j, the dimensionless group αL_j describes the in-plane foil impedance relative to the through-plane stack impedance, and determines the curvature of the foil current profiles in segment j. When $\alpha L_j \ll 1$ the through-plane stack impedance dominates the cell impedance, consequently the in-plane foil current profiles will be linear, and the through-plane stack current distribution will be close to constant. Conversely when $\alpha L_j \gg 1$ the in-plane foil impedance dominates, the foil current profiles will be curved and the through-plane stack current will be peaked at the tabs.

3.5. General solution

A solution of (8) is called the particular solution, ϕ_{p}. Any linear combination of the solutions to the homogeneous equation

$$(\nabla^2 - \alpha^2)\phi = 0 \tag{10}$$

can also be added to ϕ_{p}. When α is constant, $\exp(\pm\alpha x)$ are two linearly independent solutions to (10) and the homogenous solutions will the be same for all segments.

Anticipating the use of external current boundary conditions, for calculational convenience homogeneous solutions are calculated with unit slope at one end of a segment and zero slope at the other end of a segment, and the particular solution with zero slope at both ends. For segment j

$$\begin{aligned}
&(\nabla^2 - \alpha^2)\phi_j^{\text{left}} = 0, && \nabla\phi_j^{\text{left}}\Big|_{x=x_j} = 1, && \nabla\phi_j^{\text{left}}\Big|_{x=x_{j+1}} = 0\\
&(\nabla^2 - \alpha^2)\phi_j^{\text{right}} = 0, && \nabla\phi_j^{\text{right}}\Big|_{x=x_j} = 0, && \nabla\phi_j^{\text{right}}\Big|_{x=x_{j+1}} = 1\\
&(\nabla^2 - \alpha^2)\phi_j^{\text{p}} + \alpha^2 V_{\text{o}} = 0, && \nabla\phi_j^{\text{p}}\Big|_{x=x_j} = 0, && \nabla\phi_j^{\text{p}}\Big|_{x=x_{j+1}} = 0.
\end{aligned} \tag{11}$$

For constant α (Ohmic condition) one finds

$$\phi_j^{\text{left}} = \frac{\sinh(\alpha[x_{j+1} - x])}{\alpha\sinh(\alpha[x_{j+1} - x_j])}$$
$$\phi_j^{\text{right}} = \frac{\sinh(\alpha[x_j - x])}{\alpha\sinh(\alpha[x_{j+1} - x_j])}.$$

While analytic techniques exist for solving (11) for the Ohmic case (operator inversion methods) the resulting solution, expressed as a double integral, must be evaluated numerically. In practice it is much easier to solve (11) numerically using a tridiagonal solver.

Now the general solution for any segment can be written as

$$\phi_j = \phi_j^{\mathrm{p}} + a_j\phi_j^{\mathrm{left}} + b_j\phi_j^{\mathrm{right}}$$

where the constants a_j and b_j must be determined by boundary conditions. Due to the special properties of ϕ_{left} and ϕ_{right} the external current coming in from the left end of the segment will determine a_j and current from the right will determine b_j. Because of the special choice of boundary conditions, the physical interpretation of the particular solution, ϕ^{p}, is as follows:

- Initially when V_{o} is constant then $\phi^{\mathrm{p}} = V_{\mathrm{o}}$.
- After some current has passed V_{o} becomes non uniform. Now $\phi^{\mathrm{p}} - V_{\mathrm{o}}$ corresponds to potentials (and therefore currents) along the foils resulting only from the changes in state of charge along the length of the segment, the so called internal mixing currents [10]. Mixing currents have the interesting property that they keep running after the external current is turned off.

3.6. Electrode potentials and currents

Since all the physical boundary conditions are defined in terms of the individual electrode potentials, (ϕ_{A}, ϕ_{C}) and currents (I_{A}, I_{C}) rather than the stack potential and current, it is useful to derive expressions for the electrode potentials and currents. Using (7) and briefly dropping all segment indices one finds

$$i(x) = -\frac{\nabla^2\phi}{W(R_{\mathrm{A}} + R_{\mathrm{C}})} \tag{12}$$

and putting this into (2) and (3) and integrating one finds

$$I_{\mathrm{A}} = -W\int_{x_{\mathrm{o}}}^{x} i(x')\,\mathrm{d}x' = \frac{1}{R_{\mathrm{A}} + R_{\mathrm{C}}}\nabla\phi + I_{\mathrm{A}}(x_{\mathrm{o}}) \tag{13}$$

and

$$I_{\mathrm{C}} = W\int_{x_{\mathrm{o}}}^{x} i(x')\,\mathrm{d}x' = -\frac{1}{R_{\mathrm{A}} + R_{\mathrm{C}}}\nabla\phi + I_{\mathrm{C}}(x_{\mathrm{o}}) \tag{14}$$

where $I_{\mathrm{A}}(x_{\mathrm{o}})$ and $I_{\mathrm{C}}(x_{\mathrm{o}})$ are integration constants. One can now plug these into integrated forms of (1)

$$\begin{aligned}\phi_{\mathrm{A}} &= -R_{\mathrm{A}}\int_{x_{\mathrm{o}}}^{x} I_{\mathrm{A}}(x')\,\mathrm{d}x' \\ &= -\frac{R_{\mathrm{A}}}{R_{\mathrm{A}} + R_{\mathrm{C}}}\phi - R_{\mathrm{A}}I_{\mathrm{A}}(x_{\mathrm{o}})x + \phi_{\mathrm{A}}(x_{\mathrm{o}})\end{aligned} \tag{15}$$

and

$$\begin{aligned}\phi_{\mathrm{C}} &= -R_{\mathrm{C}}\int_{x_{\mathrm{o}}}^{x} I_{\mathrm{C}}(x')\,\mathrm{d}x' \\ &= \frac{R_{\mathrm{C}}}{R_{\mathrm{A}} + R_{\mathrm{C}}}\phi - R_{\mathrm{C}}I_{\mathrm{C}}(x_{\mathrm{o}})y + \phi_{\mathrm{C}}(x_{\mathrm{o}})\end{aligned} \tag{16}$$

Since $\phi_{\mathrm{C}}(x) - \phi_{\mathrm{A}}(x) = \phi(x)$ for all x one finds that $-R_{\mathrm{A}}I_{\mathrm{A}}(x_{\mathrm{o}}) = -R_{\mathrm{C}}I_{\mathrm{C}}(x_{\mathrm{o}}) = c$ and $\phi_{\mathrm{A}}(x_{\mathrm{o}}) = \phi_{\mathrm{C}}(x_{\mathrm{o}}) = d$. c has dimensions of electric field, i.e. (V cm^{-1}). Defining the relative foil resistances

$$r_{\mathrm{A}} = \frac{R_{\mathrm{A}}}{R_{\mathrm{A}} + R_{\mathrm{C}}} \tag{17}$$

$$r_{\mathrm{C}} = \frac{R_{\mathrm{C}}}{R_{\mathrm{A}} + R_{\mathrm{C}}} \tag{18}$$

results in

$$\phi_{\mathrm{A}} = -r_{\mathrm{A}}(\phi_{\mathrm{p}} + a\phi_{\mathrm{left}} + b\phi_{\mathrm{right}}) + cx + d \tag{19}$$

$$\phi_{\mathrm{C}} = r_{\mathrm{C}}(\phi_{\mathrm{p}} + a\phi_{\mathrm{left}} + b\phi_{\mathrm{right}}) + cx + d \tag{20}$$

$$I_{\mathrm{A}} = \frac{1}{R_{\mathrm{A}} + R_{\mathrm{C}}}(\nabla\phi_{\mathrm{p}} + a\nabla\phi_{\mathrm{left}} + b\nabla\phi_{\mathrm{right}}) - \frac{c}{R_{\mathrm{A}}} \tag{21}$$

$$I_{\mathrm{C}} = -\frac{1}{R_{\mathrm{A}} + R_{\mathrm{C}}}(\nabla\phi_{\mathrm{p}} + a\nabla\phi_{\mathrm{left}} + b\nabla\phi_{\mathrm{right}}) - \frac{c}{R_{\mathrm{C}}} \tag{22}$$

There are now four constants (a, b, c, d) which need to be determined by external boundary conditions. Each segment has its own profiles for potential and current, and therefore its own set of constants (a, b, c, d).

3.7. Boundary conditions

3.7.1. Categorizing tabs

The number of tabs for each type are defined in Table 1. The n^{i} internal tabs are located at positions x^j, $j = 1, \ldots, n^{\mathrm{i}}$. The electrode potentials above are only valid in the regions between these tabs. Right at the tabs ϕ_{A} and ϕ_{C} will be continuous but non analytic, i.e. the first derivatives, the in-plane foil currents I_{A} and I_{C}, are not always continuous. Physically the in-plane foil currents will exhibit a step change (usually changing sign as indicated by the arrows in Fig. 1) at each tab attached to that electrode. The full potential must be constructed from $n^{\mathrm{i}} + 1$ segments, so $4(n^{\mathrm{i}} + 1)$ boundary conditions are required to determine all the a_j, b_j, c_j, d_j's (using j as a segment index). The problem is now reduced to that of bookkeeping for all the boundary conditions.

3.7.2. Global boundary conditions

For the first segment, $j = 0$, one can arbitrarily set

$$\phi_{\mathrm{A}0}(0) = 0 \tag{23}$$

since only potential differences are important. Alternatively one can just set $\mathrm{d}_0 = 0$. Also the total current flowing into (or out

Table 1
Tab counting

Tab type	Internal	External	Total
Anode	$n^{\mathrm{i}}_{\mathrm{A}}$	$0 \le n^{\mathrm{e}}_{\mathrm{A}} \le 2$	$n_{\mathrm{A}} = n^{\mathrm{i}}_{\mathrm{A}} + n^{\mathrm{e}}_{\mathrm{A}} \ge 1$
Cathode	$n^{\mathrm{i}}_{\mathrm{C}}$	$0 \le n^{\mathrm{e}}_{\mathrm{C}} \le 2$	$n_{\mathrm{C}} = n^{\mathrm{i}}_{\mathrm{C}} + n^{\mathrm{e}}_{\mathrm{C}} \ge 1$
Both	n^{i}	$0 \le n^{\mathrm{e}} \le 4$	$n = n_{\mathrm{A}} + n_{\mathrm{C}} = n^{\mathrm{i}} + n^{\mathrm{e}}$

of) each electrode is fixed

$$\sum_{j\in\text{anode}}^{n_\text{A}} (I_{\text{A}j}(x_j) - I_{\text{A}j}(x_{j-1})) = -I \tag{24}$$

$$\sum_{j\in\text{cathode}}^{n_\text{C}} (I_{\text{C}j}(x_j) - I_{\text{C}j}(x_{j-1})) = I. \tag{25}$$

These two are linearly dependent, so they only count as one boundary condition. The impedance of the tab material is assumed to be negligible so the potentials of all tabs on a given electrode are all equal

$$\phi_\text{A}(x^j) = \phi_\text{A}(x^k), \quad j \neq k, \quad j,k \in \text{anode}$$

$$\phi_\text{C}(x^j) = \phi_\text{C}(x^k), \quad j \neq k, \quad j,k \in \text{cathode}.$$

There will be $n-2$ such conditions. When there are no external tabs the currents at the boundaries will all be 0

$$I_\text{A}(0) = I_\text{C}(0) = I_\text{A}(L) = I_\text{C}(L) = 0.$$

When some external tabs are present there will be $4 - n^\text{e}$ such conditions.

3.7.3. Local boundary conditions

At each of the tab positions, x_j, the potentials (but not the current) on the tabbed electrode must be joined. At the corresponding segment boundary on the opposing electrode (assuming there is no tab there) the potential *and* current must be joined. For example if there is an anode tab at x_j then both the anode and cathode potentials, and the cathode current must be joined or matched

$$\phi_{\text{C}j-1}(x_j) = \phi_{\text{C}j}(x_j) j \in \text{cathode}$$

$$\phi_{\text{A}j-1}(x_j) = \phi_{\text{A}j}(x_j) j \in \text{cathode}$$

$$I_{\text{A}j-1}(x_j) = I_{\text{A}j}(x_j) j \in \text{cathode}$$

$$\phi_{\text{A}j-1}(x_j) = \phi_{\text{A}j}(x_j) j \in \text{anode}$$

$$\phi_{\text{C}j-1}(x_j) = \phi_{\text{C}j}(x_j) j \in \text{anode}$$

$$I_{\text{C}j-1}(x_j) = I_{\text{C}j}(x_j) j \in \text{anode}.$$

There will be $3n^\text{i}$ such conditions. So in total there are

$$2 + n - 2 + 4 - n^\text{e} + 3n^\text{i} = 4 + 4n^\text{i}$$

boundary conditions as required.

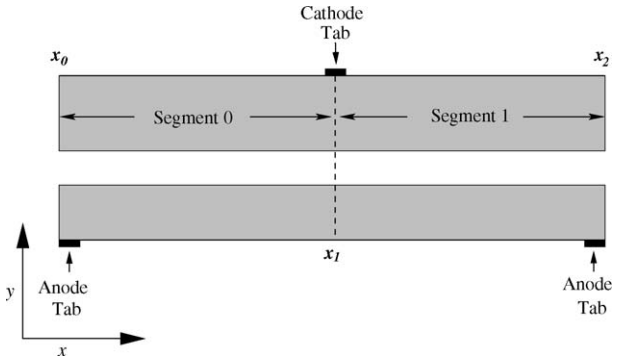

Fig. 4. Schematic showing two segments and three segment boundaries x_0, x_1 and x_2.

3.7.4. Example of boundary conditions

In order to clarify, all boundary conditions for the tab arrangement in Fig. 1 will be listed. To facilitate this, the two segments and three segment boundaries, x_0, x_1 and x_2, are shown in Fig. 4. All boundary conditions are listed in Table 2. Eqs. (19)–(22) can substituted into the relations in the last column of Table 2, to obtain a linear system of equations for $\{a_0, b_0, c_0, d_0, a_1, b_1, c_1, d_1\}$.

3.7.5. Equation system

Inserting the potential and current expressions (19)–(22) into the boundary conditions results in a system of algebraic equations for the a_j, b_j, c_j, d_j coefficients. This system can be solved manually, numerically or using symbolic algebra system, depending on the number of segments involved and the desired output. In this work the numerical approach is preferred for the following reasons:

- One must resort to numerical methods anyway for Li-ion systems where the OCV, $V_\text{o}(q)$, is a non-trivial measured function, or when the stack impedance becomes non trivial.
- I do not find the messy analytic expressions resulting from solving a two or more segment problem very enlightening.

3.8. Cell voltage and impedance

Once values for all the a_j, b_j, c_j, d_j coefficients have been determined, one can graph and interpret internal quantities, i.e. currents and potentials for both the electrode foils and the stack. These internal quantities are not very amenable to experimental

Table 2
All boundary conditions for the three tab cell design

Type	Electrode	Segment(s)	Location(s)	Condition
End current	Cathode	0	x_0	$I^0_\text{C}(x_0) = 0$
End current	Cathode	1	x_2	$I^1_\text{C}(x_2) = 0$
External current	Cathode	0, 1	x_1	$I^0_\text{C}(x_1) - I^1_\text{C}(x_1) = I$
Potential join	Cathode	0, 1	x_1	$\phi^0_\text{C}(x_1) = \phi^1_\text{C}(x_1)$
Potential join	Anode	0, 1	x_1	$\phi^0_\text{A}(x_1) = \phi^1_\text{A}(x_1)$
Current join	Anode	0, 1	x_1	$I^0_\text{A}(x_1) = I^1_\text{A}(x_1)$
Tab potentials	Anode	0, 1	x_0, x_1	$\phi^0_\text{A}(x_0) = \phi^1_\text{A}(x_2)$
Arbitrary potential	Anode	0	x_0	$\phi^0_\text{A}(x_0) = 0$

verification. This means that the calculation is the most practical method of accessing this information, but only if it is right! In order to decide one must calculate the external cell voltage and impedance and compare with experiment for a cell design for which samples or data are available.

The cell voltage is simply the potential difference between any anode tab and any cathode tab

$$V_{\text{cell}} = \phi_{\text{C}}(y_i) - \phi_{\text{A}}(y_j), \quad i \in \text{cathode}, \quad j \in \text{anode}.$$

One can define two distinct versions of cell impedance, finite difference

$$R_{\text{cell}}^{\text{fd}}(I) = \frac{V_{\text{cell}}(I=0) - V_{\text{cell}}(I)}{I}$$

and differential

$$R_{\text{cell}}^{\text{diff}} = \frac{\partial V_{\text{cell}}}{\partial I}.$$

When approximating the stack impedance as an Ohmic or constant value, these two versions of the cell impedance should be identical. It also turns out that under these conditions the cell impedance remains constant during the discharge. The finite difference version is fairly straightforward to calculate but requires one to keep track of the $I = 0$ solutions to all the equations above. Calculating the differential form requires the solution of a second system of boundary condition equations that are implicitly differentiated with respect to I. The solution yields $\partial a_j/\partial I$, $\partial b_j/\partial I$, $\partial c_j/\partial I$, $\partial d_j/\partial I$.

3.9. Foil heating

In high power applications it is essential to understand heat generation effects at high currents. Total heat is easily calculated from I^2R. However, lot of information about the cell internals is also available, which can be used to learn *where* the heat is generated. This is another effect that is very difficult to measure directly. The local heating rate in the anode foil will be

$$q_{\text{A}}(x) = \frac{1}{W_{\text{A}}} I_{\text{A}}^2 R_{\text{A}}$$

with a similar expression for the cathode. q_{A} will have dimensions of (W cm^{-2}). The local heating rate in the stack is

$$q_{\text{stack}}(x) = i^2 R_{\text{stack}}$$

with the same dimensions as q_{A}. The local heating rates can easily be integrated over space to get total heating rates, and/or over time to get total heat generated. In order to keep things as simple as possible, reversible or entropic heating (or cooling) is not included in the stack heat generation.

It is worth pointing out that since the foil currents are usually peaked near the tab positions, the heat generation rate in the foils will be even more strongly peaked near the tabs. For example even when $\alpha L \ll 1$ and the foil currents are linear, the heat generation will decay quadratically moving away from a tab. This will be shown graphically below.

3.10. Time dependence

All of the above theory describes the current and potential distributions at the instant the current is turned on. As the cell discharges all internal quantities acquire a time dependence, and the state of charge in the stack varies according to

$$q(x,t) = \int_0^t i(x,t')\,\mathrm{d}t'$$

which quickly induces non-uniformity in $V_{\text{o}}(q)$. Non-trivial effects can arise from the shape of $V_{\text{o}}(q)$. When it is flat as a function of q (voltage plateau) then large composition gradients can develop along the length of the cell (x direction). When $V_{\text{o}}(q)$ is steeply sloping, any existing composition gradients along the length will be quickly eliminated by internal mixing currents arising from ϕ_{p}.

In practice a numerical simulation is required using standard finite element methods. Results of such simulations for an $\text{Li}_x\text{Mn}_2\text{O}_4/\text{Li}_{1-x}\text{C}_6$, spiral wound Li-ion cell will be described in the next section. The goal is to demonstrate some of the interesting effects that can occur with the foil currents. For this purpose it is best to use a constant value for the stack impedance.

4. Example calculations

4.1. Cell details

Results will the shown for two cell designs using the non trivial tab arrangement shown in Fig. 1. Cell #1 is intended to be towards the power optimized end of the spectrum, and cell #2 is intended to be energy optimized. Design parameters for both cells are shown in Table 3.

The foil resistivities ρ_{A} and ρ_{C} correspond to *Cu* and *Al* respectively. The electrode widths are typical of those found in commercial 18650 size Li-ion cells. The power optimized cell (cell #1) uses thicker/longer foils and a thinner stack, which is indirectly expressed through the smaller stack resistivity. As discussed above the larger value for αL in cell #1 results in a non-linear shape for the foil currents. In order to get some significant polarization along the electrode foils, a sizeable current must be applied. In the examples below the current is 50 A of discharge current.

The OCV curve was calculated by differencing analytic approximations to $V(q)$ (described in the appendix in ref. [11]) for the anode and cathode active materials. The grid spacings $\Delta x = 0.1$ cm, $\Delta t = 0.5$ s were used. Because there are no direct comparisons to a real cell in this work, the results for V_{cell}

Table 3
Example cell designs

Parameter	Units	Cell #1	Cell #2
W_{A}	cm	5.7	5.7
T_{A}	μm	15	10
ρ_{A}	μΩ cm	1.7	1.7
R_{A}	mΩ cm^{-1}	0.20	0.30
W_{C}	cm	5.5	5.5
T_{C}	μm	20	15
ρ_{C}	μΩ cm	3.1	3.1
R_{C}	mΩ cm^{-1}	0.28	0.38
L	cm	200	100
R_{stack}	Ω cm^2	5	50
αL	–	4.60	0.86

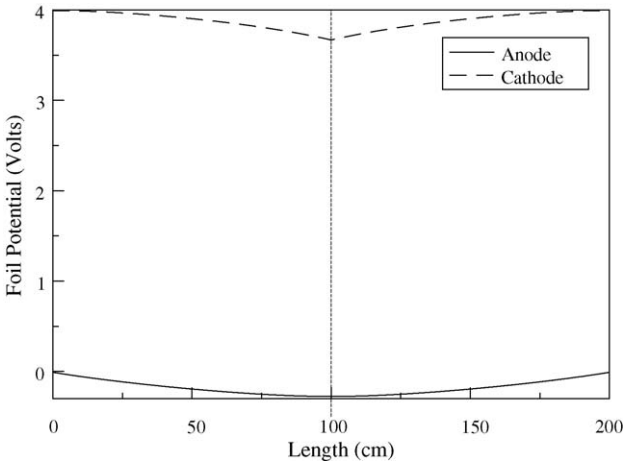

Fig. 5. Cell #1 foil potentials $\phi_A(x)$ and $\phi_C(x)$.

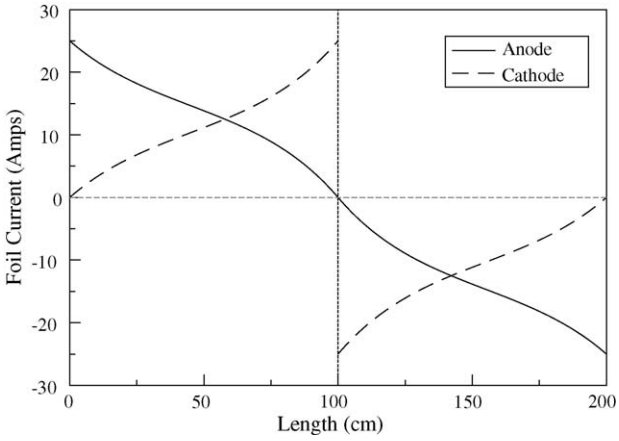

Fig. 6. Cell #1 foil currents $I_A(x)$ and $I_C(x)$.

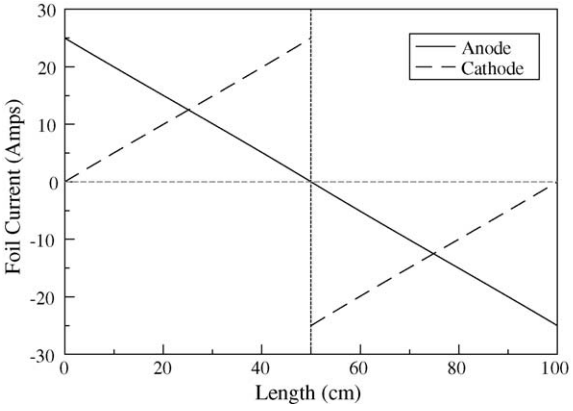

Fig. 7. Cell #2 foil currents $I_A(x)$ and $I_C(x)$.

and R_{cell} will not be discussed. Also when R_{stack} is constant their behavior is trivial.

4.2. Instantaneous results

In this section results are shown at $t = 0$, the instant the current is turned on. At this point in time the electrons are assumed to rearrange to their equilibrium charge density distribution, but no ions have moved. The calculated foil potentials for cell #1 are shown in Fig. 5. In all such figures, the vertical dashed line at $x = L/2$ indicates the position of the cathode tab. It should be remembered that anode tabs are located at the left and right edges, $x = 0$ and $x = L$. The potentials for cell #2 are qualitatively similar and are therefore not shown. The anode foil potential is highest at the tabs and exhibits a minimum half way between the two tabs. The cathode foil potential is a minimum at the tab.

The foil currents for both cells are shown in Figs 6 and 7. When viewing these graphs keep in mind that positive currents are moving to the right in Fig 1 and negative are moving to the left. Because of the symmetry in the cell designs considered, the current entering each anode tab is exactly $I/2 = 25$ A. In the case of broken symmetry, i.e. moving the cathode tab off center, the theory would tell us exactly how the current would be unevenly distributed between the two anode tabs. At the cathode tab one sees a discontinuity in the current, jumping from 25 A to −25 A. For internal tabs such current discontinuities are more the rule than the exception. One can readily see that the foil currents for cells 1 and 2 are qualitatively different. For cell #2 the currents show linear decay, as expected since αL is small, whereas the currents for cell #1 with larger αL, are noticeably non-linear. For cell #1 one can also see some asymmetry within each segment, the currents decay faster near the cathode tab because $R_C > R_A$. This asymmetry is also evident in the stack current shown in Fig. 8 which is more peaked near the cathode tab than at either anode tab.

4.3. Dynamic effects

As alluded to above the high stack current at the tab locations seen in Fig. 8, is a transitory situation. As the discharge proceeds the state of charge (SOC) becomes non-uniform as a function of x. This in turn results in a non-uniformity in the open circuit potential $V_o(q(x))$, with higher voltages away from the tabs. The voltage effect will induce in increase in the stack current away from the tabs. Finally, near the end of discharge the active material near the tabs will become used up (discharged), at which time all current must flow through the stack away from the tabs where some capacity remains. All of these effects are shown in

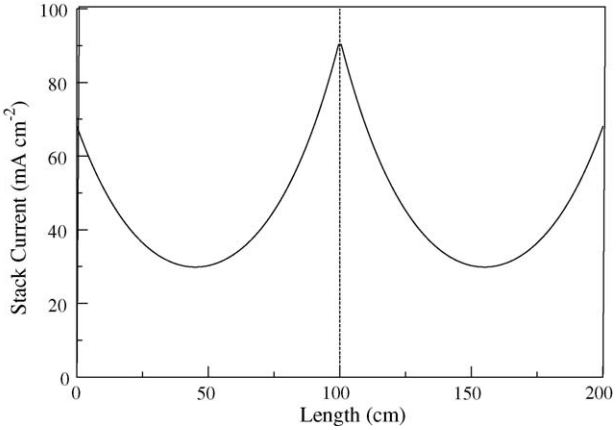

Fig. 8. Cell #1 stack current $i(x)$.

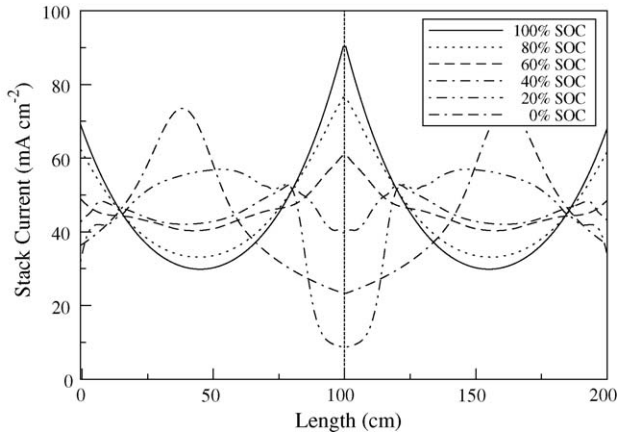

Fig. 9. Cell #1 dynamic evolution of the stack current, $i(x, t)$.

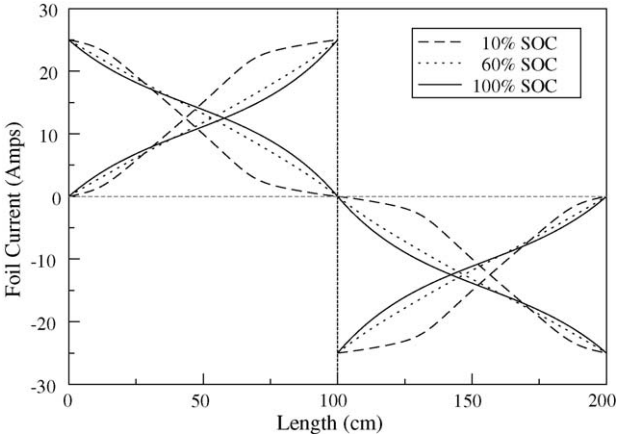

Fig. 10. Cell #1 dynamic evolution of the foil currents, $I_A(x, t)$ and $I_C(x, t)$.

Fig. 9. Some of the fine structure in these profiles is due to the non trivial shape of $V_o(q)$.

Similar effects are also observed in the foil currents (Fig. 10). In particular, at 10% SOC one can see the cathode foil running almost full current (25 A) for about 40 cm on either side of the cathode tab, before linear decay begins.

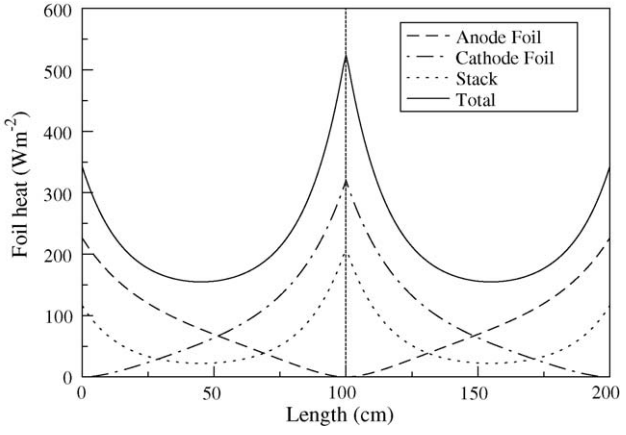

Fig. 11. Cell #1 heating generation breakdown.

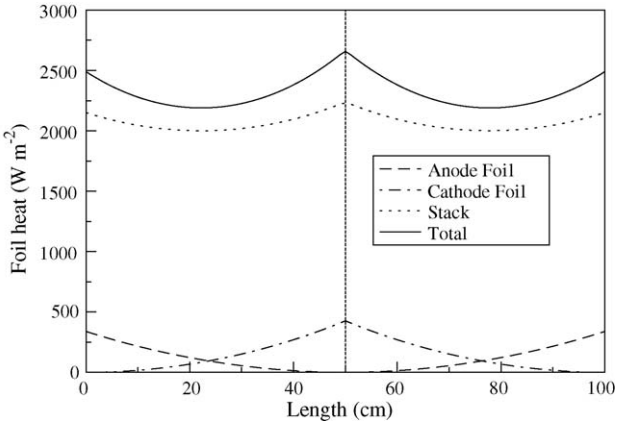

Fig. 12. Cell #2 heating generation breakdown.

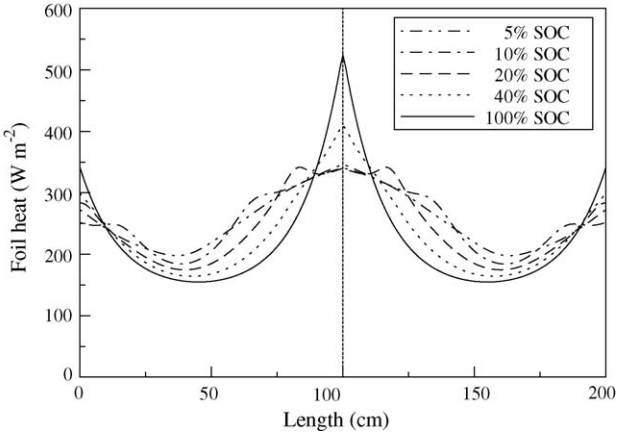

Fig. 13. Cell #1 dynamic evolution of the total heat generation.

4.4. Heating effects

A break down of various heating effects for both cells, at $t = 0$, are shown in Figs. 11 and 12. As anticipated significant heat generation is predicted near the tabs in cell #1, to which both the stack and foil contribute. Cell #1 is dominated by foil heat generation and cell #2 is dominated by more uniform stack heat generation (note the different y-axis scales). Fig. 13 gives a flavor for the time dependence of the total heat generation for the cell #1. One can see that near the end of discharge the heat generation tends to move away from the tabs, but one never observes a peak in the heating rate away from the tabs. This is just a consequence of the dominating effect of foil heating in this cell.

5. Conclusions

The purpose of this work is two-fold

(1) Outline the theory for calculating internal foil currents and potentials for a general cell design with an unlimited number of tabs, randomly located.
(2) Provide some qualitative understanding of how potentials, current and heating behaves during discharge of a cell.

In cells with low stack impedance and long electrodes, polarization effects in the foils cannot be neglected. The value of the dimensionless group αL is easily calculated, and can be used to decide if foil polarization is important for any given cell design. The degree of cell heating caused by the foils will in general depend on αL, if $\alpha L \gg 1$ the foil heating will make a major contribution, especially near the tabs. This heating will in turn change the kinetics in the stack through its dependence on electrolyte conductivity, salt diffusion, surface reaction kinetics and solid state diffusion. Taking proper account of all these interacting effects would require the incorporation of a detailed dynamic model for the stack impedance. This may be the subject of a future paper. I hope that these ideas and methods will be of assistance in designing high power cells.

Appendix A. Non Ohmic stack impedance

When the relation between the stack potential and stack current density is non-linear, then iterative methods will be required. This is always the case when a detailed stack model is used as described in ref. [1]. Because the state of charge quickly becomes non-uniform along the length of the electrodes, one must implement numerous instances of the full stack model each maintaining its own state information. The result of this is that the stack impedance now becomes non-uniform and time dependent: $R_{\text{stack}}(x, t)$. All the boundary conditions equations in (11) must be solved numerically using a tridiagonal solver.

Because i is not a small parameter, the expansion in (4) is not convergent. Given the stack current from the previous time step, or some initial guess i_o one can expand

$$i = i_o + \left.\frac{\partial i}{\partial \phi}\right|_i (\phi - \phi_o) + O(\delta\phi^2) \approx i_o - \frac{1}{R_{\text{stack}}}(\phi - \phi_o) \tag{26}$$

This corrected stack current expression can then be used in (7). The foil and stack model must be iterated until self consistency is achieved. This amounts to a decoupled two-dimensional simulation. Results of such simulations may be presented in a future publication.

References

[1] K.E. Thomas, R.M. Darling, J. Newman, Mathematical modeling of lithium batteries, in: W. van Schalkwijk, B. Scrosati (Eds.), Advances in Lithium-Ion Batteries, Kluwer Academic/Plenum Publishers, 2002, pp. 345–392.
[2] J.N. Harb, R.M. LaFollette, Mathematical model of the discharge behaviour of a spirally wound lead-acid cell, J. Electrochem. Soc. 146 (3) (1999) 809–818.
[3] D.R. Baker, M.W. Verbrugge, Temperature and current distribution in thin film batteries, J. Electrochem. Soc. 146 (7) (1999) 2413–2424.
[4] T. Yamauchi, K. Mizushima, S. Satoh, Y. Yamada, Development of a simulator for both property and safety of a lithium secondary battery, J. Power Sources 136 (2004) 99–107.
[5] M. Doyle, T. Fuller, J. Newman, Modeling of galvanostatic charge and discharge of the lithium/polymer/insertion cell, J. Electrochem. Soc. 140 (6) (1993) 1526–1533.
[6] M. Doyle, J. Newman, A.S. Gozdz, C.N. Shmutz, J.M. Tarascon, Comparison of modeling predictions with experimental data from plastic lithuim ion cells, J. Electrochem. Soc. 143 (6) (1996) 1890.
[7] J. Euler, W. Nonnenmacher, Unknown title, Electrochim. Acta 2 (1960) 268.
[8] J. Meyers, M. Doyle, R. Darling, J. Newman, The impedance response of a porous elextrode composed of intercalation particles, J. Electrochem. Soc. 147 (8) (2000) 2930–2940.
[9] I. Bloom, B.W. Cole, S.A. Sohn, J.J. Jones, E.G. Polzin, V.S. Battaglia, G.L. Henriksen, C. Motloch, R. Richardson, T. Unkelhaeuser, D. Ingersoll, H.L. Case, An accelerated calendar and cycle life study of Li-ion cells, J. Power Sources 101 (2001) 238–247.
[10] K. Thomas, J. Newman, Heats of mixing and entropy in porous insertion electrodes, J. Power Sources 119–121 (2003) 844–849.
[11] L.O. Valøen, J.N. Reimers, Transport properties of $LiPF_6$ based Li-ion battery electrolytes, J. Electrochem. Soc. 152 (5) (2005) A882–A891.